Earth and Planetary Science Letters 363 (2013) 144–155

Contents lists available at SciVerse ScienceDirect

Earth and Planetary Science Letters

journal homepage: www.elsevier.com/locate/epsl

Dynamic sulfur and carbon cycling through the end-Ordovician extinction revealed by paired sulfate–pyrite $\delta^{34}S$

David S. Jones [a,*], David A. Fike [b]

[a] Geology Department, Amherst College, Amherst, MA 01002, USA
[b] Dept of Earth & Planetary Sciences and McDonnell Center for the Space Sciences, Washington University, St. Louis, MO 63130, USA

ARTICLE INFO

Article history:
Received 5 February 2012
Received in revised form
2 August 2012
Accepted 11 December 2012
Editor: G. Henderson

Keywords:
microbial sulfate reduction
sulfur isotopes
chemostratigraphy
Anticosti Island
Hirnantian

ABSTRACT

Geochemical records of the end-Ordovician Hirnantian Stage show parallel positive excursions in the stable isotope compositions of sedimentary pyrite sulfur ($\delta^{34}S_{pyr}$), organic carbon ($\delta^{13}C_{org}$), and carbonate carbon ($\delta^{13}C_{carb}$); these isotope excursions coincide with the end Ordovician glaciation and mass extinction. A relative increase in pyrite burial (f_{pyr}) attributed to marine anoxia has been invoked to explain the sulfur isotope excursion and link oceanic redox conditions to the extinction of marine fauna. An increase in f_{pyr} would necessarily generate a parallel excursion of equal magnitude in the isotopic composition of coeval marine sulfate ($\delta^{34}S_{SO_4}$). Here we present new high-resolution paired sulfur isotope data from carbonate-associated sulfate ($\delta^{34}S_{CAS}$) and pyrite from the Hirnantian Stage of western Anticosti Island (Québec, Canada). These data document a positive 20‰ enrichment in $\delta^{34}S_{pyr}$ (comparable in magnitude to previous reports), but no parallel excursion in $\delta^{34}S_{CAS}$. This pattern provides new constraints on the origin of the $\delta^{34}S_{pyr}$ excursion and the nature of carbon–sulfur coupling through Hirnantian time. Specifically, these observations preclude enhanced pyrite burial as the cause of the Hirnantian $\delta^{34}S_{pyr}$ excursion and suggest the possible role of anoxia in the mass extinction may need to be reevaluated. Rather, the global $\delta^{34}S_{pyr}$ excursion is best explained by a transient reduction in the isotopic fractionations expressed during microbial sulfur cycling (ε_{pyr}). The ε_{pyr} record shows a strong inverse correlation with $\delta^{13}C$, suggesting a mechanistic link between carbon cycling and processes controlling ε_{pyr} during the Hirnantian. Changes in sea level or marine redox state associated with glaciation could further impact the expression of the biological fractionation (e.g., through syndepositional sediment reworking and/or chemocline migration and resultant restricted exchange of porewater sulfate). The magnitude of isotopic fractionation during microbial sulfate reduction is partially controlled by metabolic rates, which are sensitive to the abundance, type, and lability of metabolically relevant substrates. Environmental change associated with the end Ordovician glaciation may have elevated the flux of organic material to marine sediments or caused an increase in physical reworking of sediments, leading to increased microbial sulfate reduction rates and reduced ε_{pyr}. As such, the Hirnantian $\delta^{34}S_{pyr}$ excursion may be viewed as a dynamic biological response to global climate change, highlighting the connections between the carbon and sulfur biogeochemical cycles.

1. Introduction

The Hirnantian Stage of the end Ordovician Period was an interval of intense environmental and biological change. Glacial and periglacial sediments distributed across north Africa and Arabia provide evidence for the growth of an extensive continental ice sheet on south polar Gondwana (Vaslet, 1990; Ghienne, 2003; Le Heron and Dowdeswell, 2009) with multiple episodes of ice advance and retreat (Sutcliffe et al., 2000). Geochemical data and stratigraphic records from low latitude continents (Brenchley et al., 2003; Kaljo et al., 2004; Desrochers et al., 2010) suggest several cycles of glacioeustatic sea level changes, with peak glacial conditions during the Hirnantian Stage (Finnegan et al., 2011). A two-step mass extinction bounds the Hirnantian Stage, roughly associated with the beginning and end of peak glaciation (Brenchley et al., 1994, 1995; Brenchley and Marshall, 1999; Sheehan, 2001). Extinction pulses have been attributed to rapid changes in the extent of epeiric seaways during glacioeustatic sea level fluctuations and associated changes in water temperature, oxygen availability, nutrient concentrations, and availability of marine habitat (Berry and Wilde, 1978; Berry et al., 1990; Wilde et al.,

* Corresponding author. Tel.: +1 413 542 2714; fax: +1 413 542 2713.
E-mail addresses: djones@amherst.edu (D.S. Jones), dfike@levee.wustl.edu (D.A. Fike).

0012-821X/$ - see front matter © 2012 Elsevier B.V. All rights reserved.
http://dx.doi.org/10.1016/j.epsl.2012.12.015

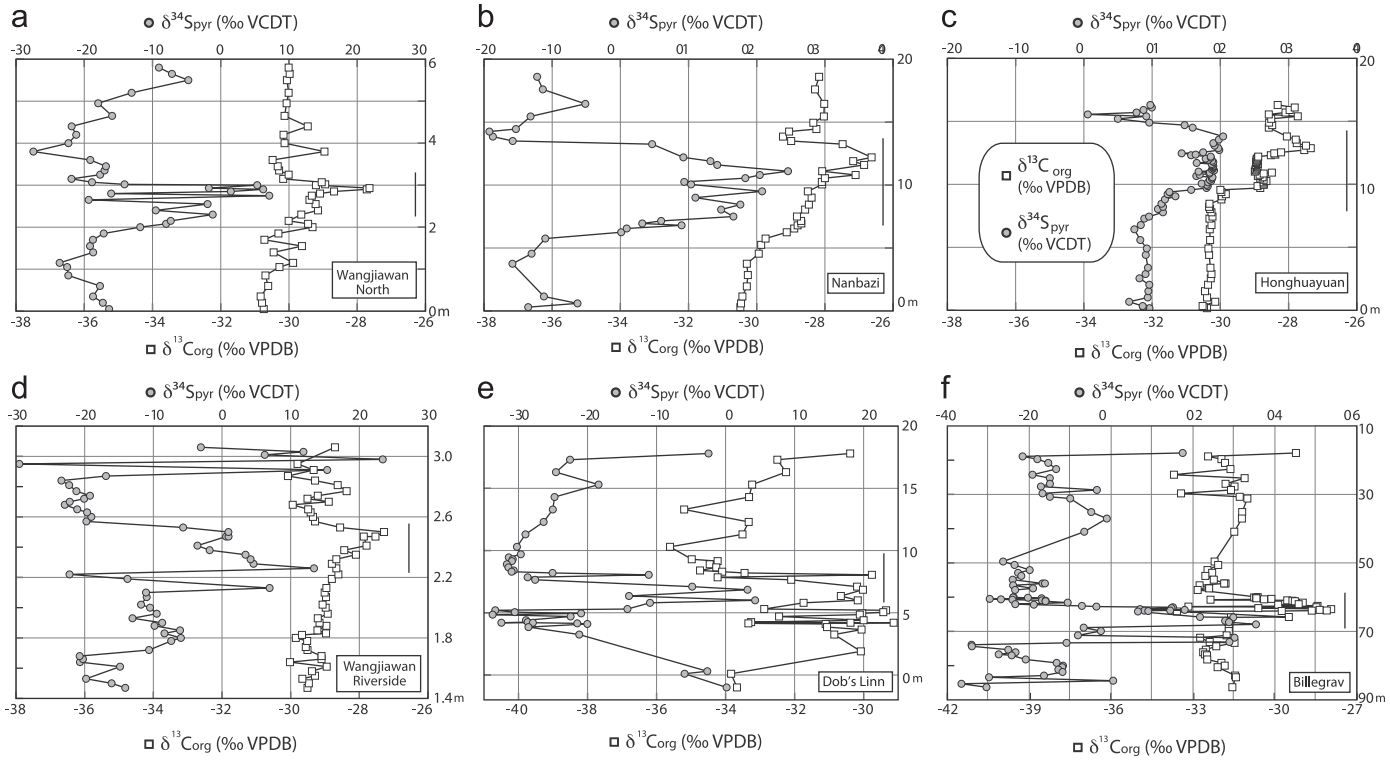

Fig. 1. Existing data from siliciclastic Hirnantian sections show parallel $\delta^{34}S_{pyr}$ and $\delta^{13}C_{org}$ excursions. (a) Wangjiawan North, South China (Yan et al., 2009). (b) Nanbazi, South China (Yan et al., 2009). (c) Honghuayuan, South China (Zhang et al., 2009). (d) Wangjiawan Riverside, South China (Gorjan et al., 2012). (e) Dob's Lin, Scotland (Hammarlund et al., 2012). (f) Bellegrav Core, Denmark (Hammarlund et al., 2012). Vertical black bars indicate extent of Hirnantian graptolite zones.

1990; Brenchley et al., 1994, 1995; Yan et al., 2009; Zhang et al., 2009; Finnegan et al., 2012b).

Hirnantian strata also contain a well-documented perturbation to the carbon cycle, recorded by a positive excursion in the stable isotopic composition of both carbonate carbon ($\delta^{13}C_{carb}$) and organic carbon ($\delta^{13}C_{org}$) (Long, 1993; Wang et al., 1993; Underwood et al., 1997; Kump et al., 1999; Brenchley et al., 2003; Kaljo et al., 2004; Young et al., 2010; Jones et al., 2011). Although the root cause of the excursion remains elusive, at least two mechanisms have been advocated: one based on increased fractional burial of organic carbon (possibly due to enhanced primary productivity stimulated by nutrient delivery associated with synglacial upwelling) (Brenchley et al., 1994, 1995); and the other based on an increase in $\delta^{13}C$ of bicarbonate delivered to the ocean by riverine runoff (due to preferential exposure and erosion of shallow carbonates vs. fossil organic matter during sea level drawdown) (Kump et al., 1999).

A ~20‰ positive excursion in the isotopic composition of sulfur in sedimentary pyrite ($\delta^{34}S_{pyr}$) occurs alongside the $\delta^{13}C$ excursion in deep marine sedimentary records from South China (Yan et al., 2009; Zhang et al., 2009; Gorjan et al., 2012), as well as Scotland and Denmark (Hammarlund et al., 2012) (Fig. 1). These records have different baseline values because the isotopic composition of pyrite is largely dependent on local processes. However, the key observation is that these $\delta^{34}S_{pyr}$ data all shift in the same direction by approximately the same magnitude at the same time, indicating a global change in sulfur cycling imprinted over locally variable conditions. These records have been interpreted to record an increase in f_{pyr} (the fraction of pyrite buried relative to total sulfur burial) driven by anoxia in deep marine basins (Zhang et al., 2009; Hammarlund et al., 2012). In these scenarios anoxic water masses are implicated as a kill mechanism for the end Ordovician mass extinction. An alternate explanation for the $\delta^{34}S_{pyr}$ excursion invokes oxygenated glacial waters that forced the chemocline deeper within sediments, resulting in limited sulfate exchange between pore waters and the overlying water column during sedimentary pyrite formation and a concomitant ^{34}S-enrichment in the resulting pyrites (Yan et al., 2009). To evaluate these hypotheses and in particular to test the interpretation that increased f_{pyr} and associated anoxia drove the sulfur isotope excursion, more information regarding the state of the ancient sulfur cycle is required.

Here we develop a quantitative framework for using time series of paired carbonate/organic carbon and carbonate-associated sulfate/pyrite isotope data to constrain processes responsible for the observed $\delta^{34}S_{pyr}$ excursion. We apply this framework to interpret parallel sulfur isotopic records of coeval carbonate-associated sulfate ($\delta^{34}S_{CAS}$) and pyrite ($\delta^{34}S_{pyr}$) in Hirnantian-aged strata from the western part of Anticosti Island, Québec. Finally we outline a new model of dynamic Hirnantian sulfur cycling based on time-varying biological fractionation. The model highlights connections between glacial climate and availability of organic substrates for microbial sulfate reduction.

2. Geological setting

Sedimentary rocks of the Ordovician–Silurian Anticosti Basin represent a subtidal, storm-influenced, carbonate ramp-platform (Petryk, 1981; Long and Copper, 1987; Sami and Desrochers, 1992; Long, 2007; Desrochers et al., 2010). The basin developed on top of Grenville-age crust on the eastern margin of Laurentia (Waldron et al., 1998). The long axis of the island is oblique to the reconstructed paleoshoreline, with the west end of the island occupying a more distal position (Petryk, 1981). Previous stratigraphic work has established several cycles of (glacio)eustatic sea level fluctuations in the Vauréal and Ellis Bay formations, interpreted to reflect the waxing and waning of continental ice sheets

on Gondwana (Desrochers et al., 2010). Subsidence of the Anticosti Basin accommodated an almost uninterrupted succession of mixed carbonate-siliciclastic strata deposited across the Ordovician–Silurian boundary despite large glacioeustatic changes in base level (Petryk, 1981; Long, 2007). Discontinuities in the $\delta^{13}C_{carb}$ record across lithostratigraphic boundaries, however, suggest that the basin experienced intermittent hiatuses in deposition during the Hirnantian Stage (Jones et al., 2011).

Here we focus on the end Ordovician (Hirnantian) Ellis Bay Formation. In particular, we present new geochemical data from the Laframboise Member of the Ellis Bay Formation, and from strata immediately below and above it, from Laframboise Point in western Anticosti Island. The stratigraphy preserved on the westernmost portion of the island has the most expanded record of Hirnantian strata on the island (Desrochers et al., 2010; Achab et al., 2011) and is independently known to host well-preserved carbonate lithologies with less diagenetic alteration than locations to the east (Finnegan et al., 2011).

3. Geochemical methods

We collected a high-resolution suite of samples from outcrop in conjunction with stratigraphic logging of the Laframboise Point section. Hand samples were slabbed with a rock saw to remove any weathered surfaces. Sulfur isotope and elemental abundance data reported here were obtained from the same sample set that yielded the carbon isotope data reported in Jones et al. (2011). Material for the elemental analyses was obtained by drilling ~100 mg of carbonate powder from each slab with a dental drill, targeting well-preserved textures (mainly fine-grained mudstones) where possible. An additional portion (~40–80 g) of each rock sample was crushed to a homogeneous powder in a Spex 8515 shatterbox with an alumina ceramic vessel for subsequent sulfate and sulfide extractions.

Approximately 30 g of powdered sample was used for each sulfate extraction, following a modified version of the procedure of Burdett et al. (1989). The powder was soaked in a 10% NaCl solution for 24 h and then rinsed three times in deionized water. It was reacted with an excess of 3 N HCl to dissolve the carbonate matrix and liberate carbonate-associated sulfate (CAS). The solution was filtered from the insoluble residue via vacuum filtration in three steps, finishing with a 0.2 μm filter. Saturated barium chloride solution was added to the filtrate to precipitate barium sulfate, which was then rinsed with deionized water and isolated by centrifugation. The resulting barium sulfate was dried overnight at 70 °C. Acid insoluble residue was rinsed with deionized water and dried at 70 °C, weighed, and then homogenized for subsequent pyrite extractions.

Insoluble residue from the CAS extraction was processed to extract pyrite sulfur using a method modified from Burton et al. (2008). Residue was placed in an airtight reaction tube along with a vial of zinc acetate solution. Air in the tube was removed under vacuum. An acidified chromium chloride solution was injected to the reaction vessel, allowing any sulfide in the residue to react to form hydrogen sulfide gas. The sulfide gas reacted with the zinc acetate solution to precipitate zinc sulfide. The resulting zinc sulfide was centrifuged, rinsed, and dried at 70 °C.

Isotopic analysis of the resulting sulfate and sulfide phases was performed using a Costech ECS 4010 elemental analyzer coupled to a Thermo Finnigan Delta V Plus mass spectrometer. For each analysis approximately 100 μg of S was loaded into a tin capsule and combusted at 1000 °C. Sulfate sample combustion was catalyzed by the addition of ~2 mg of vanadium pentoxide to the sample capsules. Evolved SO_2 gas entered the mass spectrometer in continuous flow mode. Sulfur isotope composition was calibrated against NBS-127, IAEA-S1, and IAEA-S3. Sulfur isotope values are reported in permil (‰) relative to the V-CDT (Vienna Canyon Diablo Troilite) scale. Based on replicate analyses across several days, reproducibility of sulfur isotope measurements is <0.3‰ (1σ).

Samples for elemental analysis were prepared by reacting approximately 10 mg of microdrilled carbonate powder in 10 mL of 2% acetic acid for ~6 h at 25 °C. The solution was centrifuged and then passed through a 0.2 μm filter to eliminate any fine clay fraction. Samples and blanks were then analyzed by ICP-AES using a Perkin Elmer Optima 7300DV instrument. Concentrations were determined by interpolation with a calibration curve generated from standard solutions at the time of analysis.

4. Geochemical results

Strata from Laframboise Point record the global Hirnantian carbon isotope excursion in both $\delta^{13}C_{carb}$ and $\delta^{13}C_{org}$ (Long, 1993;

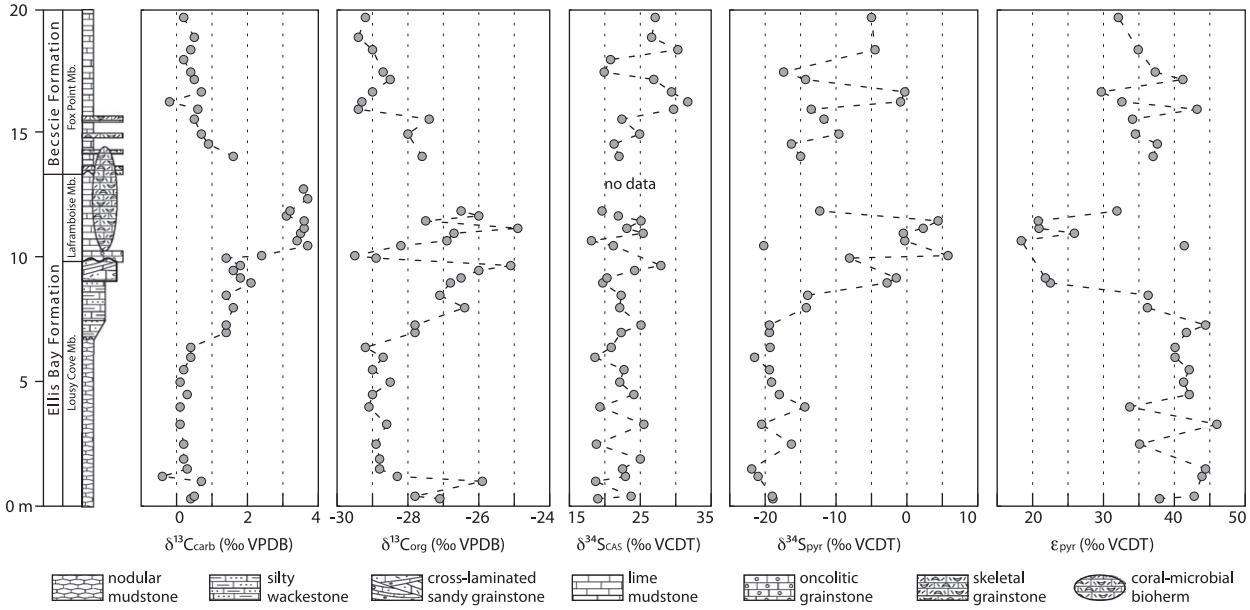

Fig. 2. Isotope ratio data from strata exposed at Laframboise Point on the western end of Anticosti Island. $\varepsilon_{pyr} = \delta^{34}S_{CAS} - \delta^{34}S_{pyr}$. Sulfur isotope ratios record a positive $\delta^{34}S_{pyr}$ excursion in parallel with excursions in $\delta^{13}C_{carb}$ and $\delta^{13}C_{org}$ without an accompanying excursion in $\delta^{34}S_{CAS}$. Carbon isotope data are from Jones et al. (2011).

Desrochers et al., 2010; Young et al., 2010; Jones et al., 2011). Here we document a parallel 20‰ enrichment in $\delta^{34}S_{pyr}$ relative to baseline (Fig. 2). The observed $\delta^{13}C$ and $\delta^{34}S_{pyr}$ excursions are confined to the upper Ellis Bay Formation and lower Becscie Formation. Although the $\delta^{34}S_{CAS}$ data show significant scatter (~5‰ variability), there is no stratigraphic trend to the data, and we observe no corresponding positive excursion in $\delta^{34}S_{CAS}$ to match that in $\delta^{34}S_{pyr}$. We also plot stratigraphic variations in ε_{pyr}, the isotopic offset between sulfate and pyrite ($=\delta^{34}S_{SO_4}-\delta^{34}S_{pyr}$), which approximates biological fractionation during sulfur cycling (Fig. 2). The coupling of the carbon and sulfur cycles can be highlighted by plotting ε_{pyr} against $\delta^{13}C_{carb}$, which yields a statistically significant inverse relationship ($r=-0.63$; $p<0.0001$; Fig. 3).

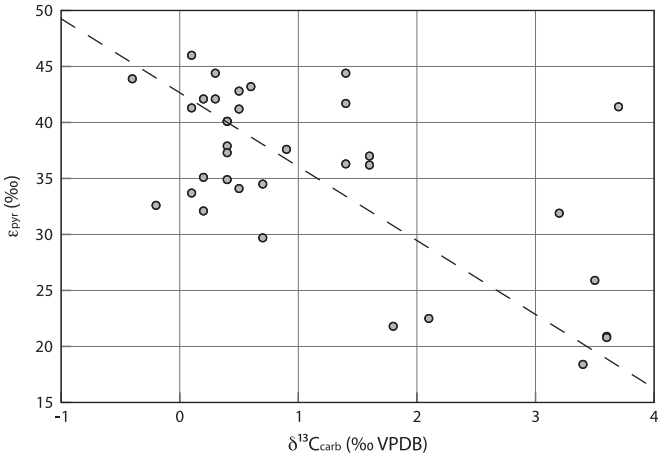

Fig. 3. Cross plot of ε_{pyr} vs. $\delta^{13}C_{carb}$, highlighting the coupling between the carbon and sulfur cycles during the Hirnantian Stage ($r^2=0.39$). Dashed line shows results of reduced major axis regression.

Isotope and elemental data (Fe/Sr, Mn/Sr, and Mg/Ca) are tabulated in Supplementary Table 1.

5. Interpretations

The positive excursion in $\delta^{34}S_{pyr}$ on western Anticosti Island (Fig. 2) is similar in magnitude (~20‰) to excursions observed in the other Hirnantian sections for which $\delta^{34}S_{pyr}$ data have been published (Yan et al., 2009; Zhang et al., 2010; Gorjan et al., 2012; Hammarlund et al., 2012), although the absolute values differ (Fig. 1). This behavior is consistent with a global change in $\delta^{34}S_{pyr}$ superimposed over locally variable conditions. The sections from South China, Scotland, and Denmark lack paired $\delta^{34}S_{CAS}$ data because the strata are not carbonate dominated. However, in these locations, the $\delta^{34}S_{pyr}$ enrichment is broadly coincident with the Hirnantian $\delta^{13}C_{org}$ excursion. Together with our data (Fig. 2), the results from these sections suggest that a Hirnantian positive excursion in $\delta^{34}S_{pyr}$ is a global phenomenon that occurs simultaneously with the perturbation to the carbon cycle (Yan et al., 2009; Zhang et al., 2010; Gorjan et al., 2012; Hammarlund et al., 2012). We use the duration of the $\delta^{34}S_{pyr}$, $\delta^{13}C_{carb}$, and $\delta^{13}C_{org}$ excursions and the $\delta^{34}S_{CAS}$ record from western Anticosti Island to place constraints on the evolution of the carbon and sulfur cycles through end-Ordovician time.

5.1. Preservation of primary isotope ratios

Carbonate minerals commonly recrystallize after burial, potentially altering their textural, geochemical, and isotopic properties (Brand and Veizer, 1980; Veizer, 1983; Given and Lohmann, 1986; Banner and Hanson, 1990; Kaufman et al., 1991). Thus, it is important to consider the possible effects that post-depositional processes may have had on the $\delta^{34}S_{CAS}$ time series data. Although considerable

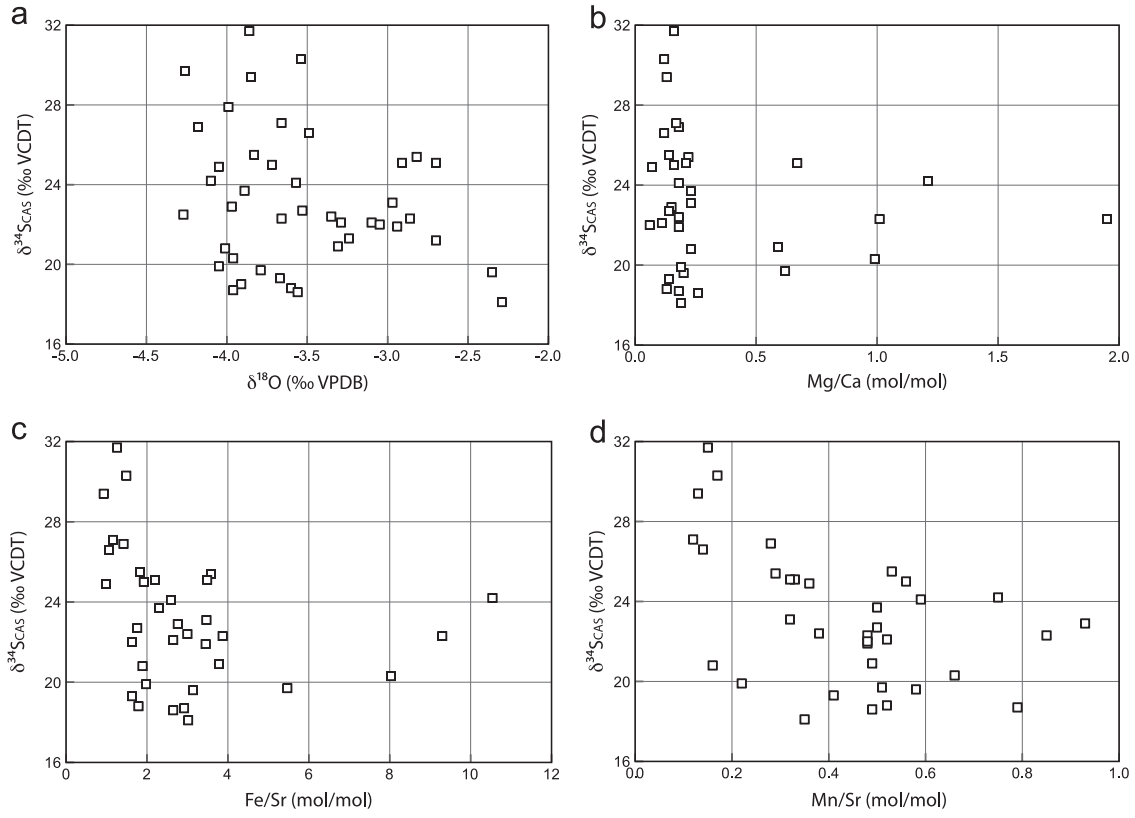

Fig. 4. Evaluation of possible diagenetic alteration to $\delta^{34}S_{CAS}$. (a) $\delta^{34}S_{CAS}$ vs. $\delta^{18}O$. (b) $\delta^{34}S_{CAS}$ vs. Mg/Ca. (c) $\delta^{34}S_{CAS}$ vs. Fe/Sr. (d) $\delta^{34}S_{CAS}$ vs. Mn/Sr.

efforts have been made to identify potential diagenetic effects on $\delta^{13}C_{carb}$ and $\delta^{18}O_{carb}$, relatively little is known about the relevant processes for $\delta^{34}S_{CAS}$. In a study of Pleistocene limestones, Gill et al. (2008) demonstrated that, although meteoric diagenesis significantly reduced CAS concentrations in aragonite that had recrystallized to low-magnesium calcite, it had little to no effect on $\delta^{34}S_{CAS}$ of the recrystallized material. Similarly, Lyons et al. (2004) showed that $\delta^{34}S_{CAS}$ of modern marine carbonate muds records $\delta^{34}S_{SO_4}$ of overlying seawater even in sediments hosting active microbial sulfate reduction (MSR) and authigenic precipitation of carbonate from the MSR-associated alkalinity flux. Despite these studies, little is known about preservation potential of $\delta^{34}S_{CAS}$ during later diagenesis and burial, and the impact of late stage pyrite oxidation cannot be fully excluded (Marenco et al., 2008a, 2008b).

Although we cannot unequivocally rule out that a $\delta^{34}S_{SO_4}$ excursion parallel to the $\delta^{34}S_{pyr}$ excursion was present in the Hirnantian ocean but not preserved in our $\delta^{34}S_{CAS}$ data, we consider it very unlikely. This observation is supported by the generally excellent preservation in the Laframboise Point samples evidenced by fossils fabrics and depositional textures (Finnegan et al., 2011). The diagenetic masking of a 20‰ excursion in $\delta^{34}S_{CAS}$ would have required stratigraphically varying amounts of sulfide oxidation and carbonate recrystallization. However, the $\delta^{34}S_{CAS}$ data show little to no covariation with a suite of standard diagenetic proxies, suggesting they are little altered (Fig. 4). The $\delta^{34}S_{CAS}$ of the Anticosti samples does not covary with $\delta^{18}O_{carb}$ ($r^2=0.06$) (Fig. 4a), a common proxy for geochemical alteration during recrystallization. The Anticosti samples are minimally dolomitized, and $\delta^{34}S_{CAS}$ shows no correlation with Mg/Ca ($r^2=0.02$), even for two samples with anomalously high (>1) Mg/Ca ratios (Fig. 4b). A weak inverse relationship exists between $\delta^{34}S_{CAS}$ and Fe/Sr ($r^2=0.07$, rising to $r^2=0.24$ if 3 anomalous samples with Fe/Sr >6 are excluded) (Fig. 4c) and Mn/Sr ($r^2=0.24$) (Fig. 4d). The exact process(es) that may lead to diagenetic alteration of $\delta^{34}S_{CAS}$ are not clear. It is possible that different amounts of carbonate recrystallization, leading to variations in Fe/Sr and Mn/Sr, also allowed sulfate impacted by pyrite oxidation to be incorporated into the carbonate matrix, resulting in the ~5‰ scatter in the $\delta^{34}S_{CAS}$ data. However, it is unlikely that this alteration would reset the $\delta^{34}S_{CAS}$ record entirely, masking the presence of a 20‰ $\delta^{34}S_{CAS}$ excursion. Further, the massive remobilization of sulfide needed to alter the $\delta^{34}S_{CAS}$ signature would likely have also altered the $\delta^{34}S_{pyr}$ record; yet the $\delta^{34}S_{pyr}$ record preserves the expected 20‰ excursion (Fig. 2).

An examination of the relationship between sulfur isotope ratios and the carbon isotope excursion provides additional support for the fidelity of the $\delta^{34}S_{CAS}$ record. Specifically, the relationship between $\delta^{13}C_{carb}$ and biological fractionation of sulfur (ε_{pyr}) is somewhat stronger ($r^2=0.39$, Fig. 3) than the relationship between $\delta^{13}C_{carb}$ and $\delta^{34}S_{pyr}$ ($r^2=0.28$, not plotted). Because any post-depositional alteration of the $\delta^{34}S_{CAS}$ signal would have impacted ε_{pyr} but not $\delta^{34}S_{pyr}$, the stronger relationship between $\delta^{13}C_{carb}$ and ε_{pyr} suggests that $\delta^{34}S_{CAS}$ was not significantly altered after pyrite formation. Thus, it is very unlikely that diagenesis could have overprinted a primary $\delta^{34}S_{CAS}$ excursion. In summary, we believe that the trends in the observed $\delta^{34}S_{CAS}$ and $\delta^{34}S_{pyr}$ records accurately represent Hirnantian sulfur cycling in the Anticosti basin (Fig. 2) and globally (Fig. 1).

5.2. Timescale

In order to discriminate between possible mechanisms of secular isotopic change, the rates of change must be adequately constrained. The $\delta^{34}S_{pyr}$ excursion documented in South China spans the two graptolite zones of the Hirnantian Stage, the older *N. extraordinarius* and the younger *N. persculptus* (Yan et al., 2009; Zhang et al., 2009). The most comprehensive work on the Ordovician time scale, based on constrained optimization of biostratigraphic and radiometric data, has yielded a duration for the Hirnantian Stage of 1.27 Ma, running from 444.68 Ma to 443.41 Ma (Sadler et al., 2009).

Siliciclastic Hirnantian sections, including the Hirnantian GSSP at Wangjiawan (South China) and the Silurian GSSP at Dob's Linn (Scotland), have well-established relative chronologies due to the good abundance and preservation of biostratigraphically useful fauna, especially graptolites. Yet, in order to develop a more complete record of biogeochemical cycling (e.g., including isotope records for $\delta^{13}C_{carb}$ and $\delta^{34}S_{CAS}$), carbonate-rich successions like those at Laframboise Point are crucial. However, the duration of the $\delta^{34}S_{pyr}$ excursion documented on western Anticosti Island is difficult to constrain in absolute terms due to uncertainties in global correlation brought about by an ambiguous biostratigraphic record. The graptolite record on Anticosti Island has been the subject of considerable debate (Riva, 1988; Underwood et al., 1997; Brenchley et al., 2003; Melchin, 2008). This record and other paleontological data (brachiopods, chitinozoans, acritarchs) have been used to argue that the entire Ellis Bay Formation is of Hirnantian age (Copper, 1999; Delabroye and Vecoli, 2010; Achab et al., 2011; Delabroye et al., 2011), with the Laframboise Member representing a single cycle of glacioeustatic sea level change. If correct, this would imply that the excursions documented in Fig. 3 took place on a timescale considerably shorter than 1.27 Ma. An alternate interpretation of the $\delta^{13}C_{carb}$ record places the base of the Hirnantian Stage at the base of the Laframboise Member of the Ellis Bay Formation (Underwood et al., 1997; Brenchley et al., 2003; Kaljo et al., 2008; Hints et al., 2010; Jones et al., 2011), which would suggest the duration of the excursions is approximately 1.27 Ma. Without endorsing a particular perspective on the chronostratigraphy of western Anticosti Island, it is clear that the duration of the excursion was greater than 150 kyr but shorter than 1.5 Myr. This time range shapes the available solution space of end Ordovician sulfur cycle processes that we explore with isotope mass balance calculations.

5.3. Modeling Hirnantian $\delta^{34}S$ variability

Isotopic mass balance in the sulfur cycle is often described using the following steady-state notation:

$$\delta^{34}S_{in} = \left(1-f_{pyr}\right) \times \delta^{34}S_{SO_4} + f_{pyr} \times \delta^{34}S_{pyr} \quad (1)$$

where f_{pyr} is the fraction of sulfur buried as pyrite relative to the sum of sulfate and pyrite burial, and $\delta^{34}S_{in}$ is the isotopic composition of sulfur entering the ocean. This can be rewritten as:

$$\delta^{34}S_{SO_4} = \delta^{34}S_{in} + f_{pyr} \times \varepsilon_{pyr} \quad (2)$$

by substituting $\varepsilon_{pyr}=\delta^{34}S_{SO_4}-\delta^{34}S_{pyr}$ to represent the biological fractionation during microbial sulfur cycling. This formulation emphasizes the three parameters that are thought to play a major role in the long-term evolution of the sulfur cycle (ε_{pyr}, f_{pyr}, $\delta^{34}S_{in}$). Importantly, Eq. (2) also makes clear the fact that two of these mechanisms (f_{pyr} and $\delta^{34}S_{in}$) affect sulfur isotope ratios by altering the sulfur isotopic composition of marine sulfate. The resulting isotopic signal is subsequently incorporated into the $\delta^{34}S_{pyr}$ record differently depending on which parameter in the sulfur cycle changes. For a change in f_{pyr} or $\delta^{34}S_{in}$, both $\delta^{34}S_{SO_4}$ and $\delta^{34}S_{pyr}$ move in the same direction and by the same magnitude. However, for a change in ε_{pyr}, $\delta^{34}S_{SO_4}$ and $\delta^{34}S_{pyr}$ change in different directions, with the magnitude of their changes depending on f_{pyr}; for a unit increase in ε_{pyr}, $\delta^{34}S_{SO_4}$ increases by $\varepsilon_{pyr} \times f_{pyr}$, while $\delta^{34}S_{pyr}$ decreases by $\varepsilon_{pyr} \times (1-f_{pyr})$. It is important to remember that these patterns reflect the 'steady-state' results obtained after the system has re-equilibrated

in response to a one-time shift in the parameters governing sulfur cycling.

In the case of secular variation in Hirnantian sulfur cycling, however, we are inherently seeking a time-dependent mechanism. As such, we need to recast Eq. (2) to include temporal evolution of the sulfur cycle:

$$\frac{d}{dt}\left[\delta^{34}S_{SO_4}\right] = \frac{F_{in}\left(\delta^{34}S_{in}-\delta^{34}S_{SO_4}\right)-f_{pyr}*F_{out}\left(\delta^{34}S_{pyr}-\delta^{34}S_{SO_4}\right)}{M} \quad (3)$$

where M is the size of the marine sulfate reservoir (moles) and F_{in} and F_{out} are the sulfur fluxes (moles/year) into and out of the ocean, respectively. Note that in Eq. (3), we are implicitly assuming there is no fractionation between the seawater sulfate reservoir and the sulfate-containing minerals (e.g., evaporites or carbonate-associated sulfate) that precipitate from it. Eq. (3) can be further simplified by assuming mass balance (i.e., the flux into and out of the ocean are equal):

$$\frac{d}{dt}\left[\delta^{34}S_{SO_4}\right] = \frac{F_s}{M}\times\left(\left(\delta^{34}S_{in}-\delta^{34}S_{SO_4}\right)+f_{pyr}\times\varepsilon_{pyr}\right) \quad (4)$$

where $F_s=F_{in}=F_{out}$. The assumption of mass balance limits the range of solutions we explore for the end Ordovician sulfur cycle, and future studies may refine our results by considering models in which the size of the sulfate reservoir (M) changes over time due to imbalances in F_{in} and F_{out} (Wortmann and Chernyavsky, 2007; Halevy et al., 2012; Wortmann and Paytan, 2012). However, the fundamental results of our modeling efforts would remain valid even if the assumption of mass balance were relaxed (see discussion in Section 5.4.1).

In considering possible causative mechanisms, we set the duration of the Hirnantian Stage to be 1.5 Myr; this is a conservative upper bound for the duration of the excursions at Laframboise Point (see Section 5.2). For modeling the mass flux of the sulfur cycle, we use a baseline sulfate concentration of 7.5 mM, based on fluid-inclusion estimates from Cambrian (5–11 mM) and Silurian (5–12 mM) evaporites (Lowenstein et al., 2003) and values of F_S centered around modern values of 3×10^{12} mol/yr (Kah et al., 2004). To test the sensitivity of the model results to these parameters, we explore varying sulfate concentrations from 5 to 10 mM and F_S from 2×10^{12} to 1×10^{13} mol/yr. For modeling isotopic evolution, we use the following as baseline values: $\delta^{34}S_{in}=10‰$, $f_{pyr}=0.25$, and $\varepsilon_{pyr}=40‰$, which are chosen to approximate the Ordovician sulfur cycle as best as is currently known (Canfield, 2004; Kampschulte and Strauss, 2004; Fike and Grotzinger, 2008).

We employ Eq. (4) to examine possible causative mechanisms for the observed Hirnantian sulfur isotope record. The absence of a parallel excursion in $\delta^{34}S_{CAS}$ accompanying the 20‰ positive excursion in $\delta^{34}S_{pyr}$ on Anticosti Island illustrates that the perturbation to sulfur cycling did not involve change in the parent marine sulfate reservoir itself. Thus, in seeking to reconstruct Hirnantian sulfur cycling, we are explicitly looking for processes that (1) can generate substantial (~20‰) enrichments in $\delta^{34}S_{pyr}$ on the relatively short timescales (10^5–10^6 yr) represented by the Hirnantian Stage and yet (2) do not result in a corresponding change in $\delta^{34}S_{SO_4}$. We do not necessarily seek to reproduce the absolute values of the Anticosti sulfur isotope record; rather, we are interested in processes that reproduce the direction and magnitude of change (or lack thereof) in

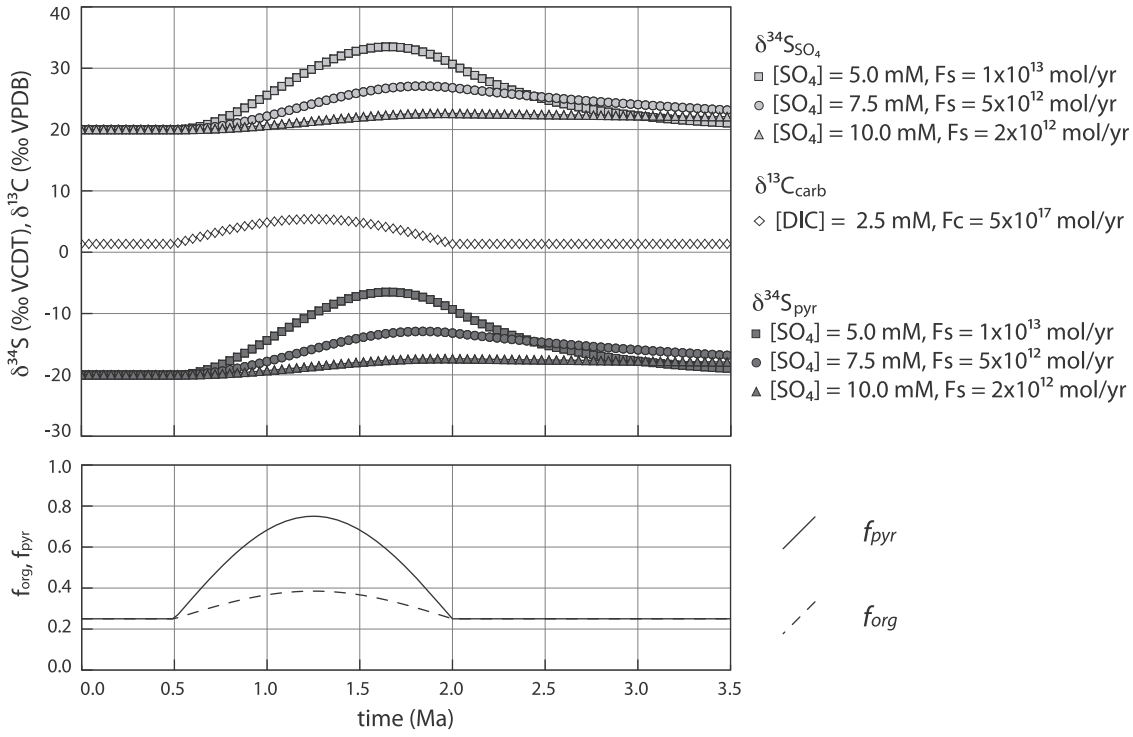

Fig. 5. Model of dynamic $\delta^{13}C_{carb}$, $\delta^{34}S_{SO_4}$, and $\delta^{34}S_{pyr}$ variation in response to a parallel pulse of enhanced carbon (f_{org}) and pyrite (f_{pyr}) burial spanning the Hirnantian Stage. Variations in f_{org} and f_{pyr} are parameterized as sinusoidal, increasing from baseline values of 0.25 to peaks of 0.75 for f_{pyr} and 0.38 for f_{org}, and return to 0.25 after 1.5 Myr. Carbon cycle perturbation assumes $\delta^{13}C_{in}=-6‰$, marine DIC=2.5 mM; and F_C=2e15 mol/yr. S cycle perturbations assume $\delta^{34}S_{in}=10‰$. The impact of variable sulfate concentrations ([SO_4]) and input flux (F_S) are represented by the three different model runs (see legend). Realistic estimates of S cycle parameters (triangle symbol) preclude any substantial variation in $\delta^{34}S_{pyr}$ or $\delta^{34}S_{SO_4}$. Liberal selection of S cycle parameters (square) can create the desired $\delta^{34}S_{pyr}$ excursion but also generates a parallel $\delta^{34}S_{SO_4}$ excursion, which is not seen in the data (Fig. 2). Note, in all cases, there is a substantial time lag between the peaks in $\delta^{34}S_{pyr}$ and $\delta^{13}C$ that is not seen in the existing data (Figs. 1 and 2). Significant decoupling between fractional burial of organic carbon and pyrite would be required to achieve the observed magnitudes of change in $\delta^{34}S_{pyr}$ and $\delta^{13}C$.

simultaneously resolved $\delta^{34}S_{CAS}$ and $\delta^{34}S_{pyr}$ records at the appropriate time scale.

5.3.1. Varying f_{pyr} or $\delta^{34}S_{in}$

We first attempt to explain the observed $\delta^{34}S$ record by invoking increased pyrite burial; this is a test of the hypothesis advanced to explain the positive $\delta^{34}S_{pyr}$ excursions from sections in South China (Fig. 1) (Zhang et al., 2009). As noted by Zhang et al. (2009), enhanced pyrite burial "would have driven enrichment of ^{34}S for seawater sulfate in the Hirnantian oceans." Using plausible parameters for sulfur cycling ($[SO_4]=7.5$ mM; $F_S=2\times10^{12}$ mol/yr), it is not possible to generate a 20‰ $\delta^{34}S_{pyr}$ within the time constraints of the Hirnantian even using a 200% increase in pyrite burial (increasing f_{pyr} from 0.25 to 0.75) (Fig. 5). Even with the most liberal parameters examined ($[SO_4]$ of 5 mM and input/output fluxes three times higher than the present), we are unable to generate a $\delta^{34}S_{pyr}$ excursion comparable to that observed in Hirnantian strata (Figs. 1 and 2). In the likely case that the Hirnantian $\delta^{34}S_{pyr}$ excursion took less time than our conservative estimate, an f_{pyr}-based explanation would be even less plausible.

Furthermore, by forcing f_{pyr}, a positive excursion in $\delta^{34}S_{SO_4}$ will always accompany the $\delta^{34}S_{pyr}$ excursion (Fig. 5). Indeed, mechanistically it is the isotopic enrichment in the source sulfate that is the cause for the parallel increase in $\delta^{34}S_{pyr}$ when f_{pyr} is increased. If sulfate concentrations were sufficiently low ($\sim$1 mM), as suggested for the early Paleozoic by some authors based on stratigraphic variability in $\delta^{34}S$ records (e.g., Hurtgen et al., 2009; Gill et al., 2011; Loyd et al., 2012), then a $\delta^{34}S_{pyr}$ excursion of the requisite magnitude could be generated; however, a parallel excursion in $\delta^{34}S_{SO_4}$ would also result, and such a coeval $\delta^{34}S_{CAS}$ excursion is not seen in the paired data from Anticosti Island (Fig. 2). Thus, for the most likely choice of environmental parameters, there is insufficient time for an excursion in $\delta^{34}S_{pyr}$ (or $\delta^{34}S_{SO_4}$), whereas when parameters are pushed to their limits to generate an excursion in $\delta^{34}S_{pyr}$, a parallel excursion in $\delta^{34}S_{SO_4}$ is also generated, counter to what is observed in the rock record.

To summarize, there is no plausible mechanism based on changing f_{pyr} to generate the observed isotopic record of $\delta^{34}S_{pyr}$ and $\delta^{34}S_{CAS}$ on the appropriate timescale. By inspection of Eq. (4), it is clear that this problem (i.e., a parallel $\delta^{34}S_{SO_4}$ excursion) also plagues any attempt to explain the Hirnantian $\delta^{34}S$ data by invoking temporal variation in $\delta^{34}S_{in}$. Variable $\delta^{34}S_{in}$ was also independently rejected by Hammarlund et al. (2012) based on the required magnitude of change in the $\delta^{34}S_{in}$ flux necessary to drive the Hirnantian $\delta^{34}S_{pyr}$ excursion.

5.3.2. Varying ε_{pyr}

Unlike scenarios based on changes in f_{pyr} or $\delta^{34}S_{in}$, explanations for the observed $\delta^{34}S$ pattern of Hirnantian sulfur cycling based on changes in biological fractionation (ε_{pyr}) appear promising. The appeal of varying the biological fractionation during microbial sulfur cycling is that the impact on $\delta^{34}S_{pyr}$ could be as fast as the changes in ε_{pyr} (i.e., changes are not slowed by the response time of the marine sulfate reservoir, which precluded f_{pyr}- or $\delta^{34}S_{in}$-based explanations) and that these changes explicitly impact the $\delta^{34}S_{pyr}$ and $\delta^{34}S_{SO_4}$ records differentially. Fig. 6 shows the impact of a sinusoidal decrease in ε_{pyr} from 40‰ to 20‰ and back to 40‰ over 1.5 Myr. Initially, the change in $\delta^{34}S_{pyr}$ corresponds exactly to the induced variation in ε_{pyr}. Superimposed on the rapid change in $\delta^{34}S_{pyr}$ associated with varying ε_{pyr}, a slower response is also seen whereby $\delta^{34}S_{SO_4}$ and $\delta^{34}S_{pyr}$ gradually decrease in response to a drop in ε_{pyr} (approaching their expected steady-state values). The magnitude of this latter variation is dwarfed by the variation in $\delta^{34}S_{pyr}$ that occurs

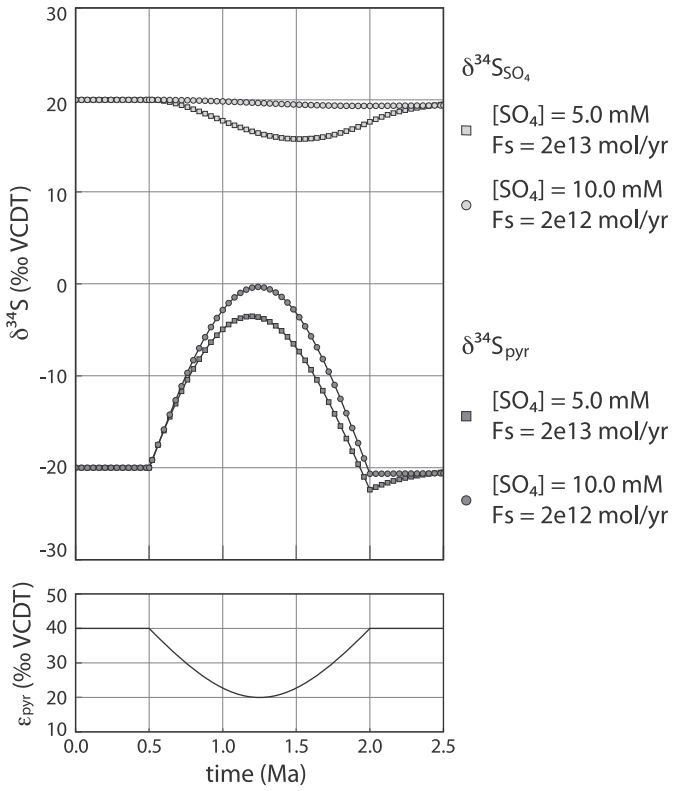

Fig. 6. Model of dynamic $\delta^{34}S_{SO_4}$ and $\delta^{34}S_{pyr}$ variation in response to a sinusoidal decrease in ε_{pyr} from baseline values of 40‰ to a minimum of 20‰ and back to 40‰ after 1.5 Myr. S cycle perturbations assume $\delta^{34}S_{in}=10$‰. The impact of variable sulfate concentrations ($[SO_4]$) and input flux (F_S) are represented by the two different model runs (see legend). For plausible parameterization, a 20‰ decrease in ε_{pyr} generates a positive excursion in $\delta^{34}S_{pyr}$ without a corresponding $\delta^{34}S_{SO_4}$ excursion, as seen in our data (Fig. 2). Even with very liberal S cycle parameters, only a small ($\sim$5‰) negative excursion in $\delta^{34}S_{SO_4}$ can be generated.

synchronously with variation in ε_{pyr} (Fig. 6). This offset highlights the importance of dynamic vs. quasi-static (i.e., 'steady-state') changes in the sulfur cycle on timescales relevant to Hirnantian sulfur cycling (and events of similar duration throughout Earth history). Thus, an environmental perturbation that resulted in a 20‰ decrease in ε_{pyr} could explain the observed Hirnantian $\delta^{34}S_{pyr}$ excursion and, at the same time, would not generate a corresponding $\delta^{34}S_{SO_4}$ excursion of comparable magnitude. Because the isotopic response of $\delta^{34}S_{pyr}$ to change in ε_{pyr} is immediate, this process could also generate the $\delta^{34}S_{pyr}$ excursion at Laframboise Point even if the duration were significantly less than 1.5 Myr.

This mechanism requires a global shift in ε_{pyr}, a parameter that is most often thought to reflect local conditions. We suggest, however, that it is possible for a global environmental change (e.g., glaciation of Gondwana) to act as a trigger that produces similar environmental responses worldwide. These responses would lead to synchronous and sympathetic shifts in ε_{pyr} across the globe. *These global trends in ε_{pyr} would be superimposed over its locally variable values, such that globally averaged ε_{pyr} could change coherently over time.* Indeed, this is what is seen in the existing Hirnantian $\delta^{34}S_{pyr}$ records, which all show an excursion of similar magnitude superimposed over locally variable baseline $\delta^{34}S_{pyr}$ values (Figs. 1 and 2).

The idea of secular variations in ε_{pyr} is not inherently novel; it is well known from globally averaged compilations that ε_{pyr} has undergone pronounced secular variation, increasing from near zero in the Archean to $\sim$25‰ over much of the Proterozoic, and

further to values in excess of 55‰ in the Phanerozoic (Canfield, 2001a). Even within the Phanerozoic, there is evidence for substantial secular changes in ε_{pyr} (Canfield, 2004). Analogous variation in the biological fractionation during carbon cycling are also observed over the geologic record (Hayes et al., 1999). However, the changes in ε_{pyr} invoked here are on a much finer time-scale, occurring over 10^5–10^6 yr, rather than 10^7–10^8 yr.

5.4. Potential biogeochemical mechanisms for Hirnantian variations in ε_{pyr}

Having established that a global change in ε_{pyr} is of the right magnitude and timing to generate the observed 20‰ positive excursion in Hirnantian $\delta^{34}S_{pyr}$ (without generating a parallel excursion in $\delta^{34}S_{SO_4}$), we now seek possible environmental and/or ecological changes that could create such a substantial change in ε_{pyr}—and one that could be global in effect. There are many factors that contribute to ε_{pyr} in natural biological systems (Habicht and Canfield, 1997; Habicht et al., 1998, 2002; Canfield, 2001b, 2001a; Canfield et al., 2006; Sim et al., 2011a, 2011b), which we briefly outline below.

5.4.1. Sulfate concentration

Ambient sulfate concentration is commonly invoked to explain variation in ε_{pyr} during microbial sulfate reduction (MSR). Specifically, laboratory experiments have shown that sulfate concentrations below ~200 μM often result in small or zero values for ε_{pyr}, which increases to values ~25–40‰ for non-limiting sulfate concentrations, holding all other parameters constant (Habicht et al., 2002). However, in natural environments much larger fractionations can be observed even under low sulfate concentrations (e.g., Canfield et al., 2010), suggesting that metabolic rates rather than sulfate availability itself may underlie this relationship.

The size of the marine sulfate reservoir is believed to have changed dramatically over Earth history (Brennan and Lowenstein, 2002; Kah et al., 2004; Wortmann and Chernyavsky, 2007; Halevy et al., 2012; Wortmann and Paytan, 2012), and changes in marine sulfate concentrations have been invoked to explain stratigraphic changes in ε_{pyr} over multi-million year time scales (Fike et al., 2006). However, in order for a changing sulfate reservoir to impact biological fractionation such that it drove the changes in ε_{pyr} observed here, the marine sulfate reservoir would have had to shrink by an order of magnitude and then return to its previous size, all within Hirnantian time. The time scale of the observed ε_{pyr} excursion is sufficiently short, however (see discussion in Section 5.2), to make this scenario unlikely.

Moreover, a change in marine sulfate concentrations would have a more direct impact on $\delta^{34}S_{SO_4}$ than that resulting from sulfate-dependent fractionation. If the absolute flux of sulfur (sulfate + sulfide) out of the ocean is larger than the incoming flux, seawater $\delta^{34}S_{SO_4}$ will increase as the marine sulfate reservoir shrinks (holding f_{pyr}, the relative proportion of pyrite and sulfate burial, constant); conversely, if the flux into the ocean is larger (i.e., marine $[SO_4]$ increases), then $\delta^{34}S_{SO_4}$ will decrease. However, this process does not change the isotopic fractionation during microbial sulfur cycling and therefore will induce parallel variations in $\delta^{34}S_{SO_4}$ and $\delta^{34}S_{pyr}$, just as the aforementioned scenario for changing f_{pyr}. Thus, a time-varying sulfate reservoir in and of itself does not capture the behavior of the paired $\delta^{34}S_{CAS}$ and $\delta^{34}S_{pyr}$ records for the Hirnantian at Laframboise Point.

5.4.2. Oxidative portion of microbial sulfur cycling

The magnitude of ε_{pyr} can also be impacted by changing the types and relative activity of the different microbial metabolisms that together comprise sulfur cycling (e.g., MSR, sulfide oxidation, and sulfur disproportionation). For example, the addition of sulfide oxidation and disproportionation can result in a substantial increase in ε_{pyr} relative to environments characterized primarily by MSR (Canfield and Teske, 1996). In modern microbial environments, the presence of disproportionation has been invoked to explain increases in ε_{pyr} on the order of ~20–30‰ (Canfield and Teske, 1996; Canfield et al., 1998; Habicht et al., 1998). Increases in the occurrence of disproportionation have also been invoked to explain substantial increases in ε_{pyr} in many key geobiological intervals of Earth history (Canfield and Teske, 1996; Fike et al., 2006; Parnell et al., 2010), although the types of metabolic activity and environmental relevance can only be inferred from the rock record.

We consider the possibility that secular changes in disproportionation and sulfur oxidation caused the observed changes in ε_{pyr}. In order to do so we need information regarding the redox state of the Hirnantian ocean. The syn-glacial ocean is often viewed as having been well-ventilated, although much of the evidence is indirect (Brenchley et al., 1995; Poussart et al., 1999; Pope and Steffen, 2003; Herrmann et al., 2004). Recent work has taken advantage of geochemical redox proxies such as iron speciation and molybdenum abundance. Iron speciation data from South China have been used to argue for a stratified redox model (oxic on top, ferruginous at depth) for the Late Ordovician–Early Silurian, punctuated by a fully oxic water column during the Hirnantian (Yan et al., 2012). Notably, these oxic intervals coincide with the $\delta^{34}S_{pyr}$ excursion (Yan et al., 2009). Outside of South China, the section with the best resolved $\delta^{34}S_{pyr}$ excursion that also has published iron speciation data is the Billegrav core from Denmark (Hammarlund et al., 2012). Here the iron speciation and paleontology also point to oxic depositional conditions during the $\delta^{34}S_{pyr}$ excursion (and maximum glacioeustatic sea level drawdown), with anoxic depositional conditions before and after the Hirnantian (Hammarlund et al., 2012).

At Laframboise Point, the ε_{pyr} excursion is directly associated with peak glacial conditions and a drop in tropical sea surface temperatures (Finnegan et al., 2011) as measured by the carbonate clumped isotope paleothermometer (Ghosh et al., 2006). The samples that yielded the coldest paleo-ocean temperatures and highest values for $\delta^{18}O_{seawater}$—indicating the Hirnantian glacial maximum—are from the same stratigraphic section and interval at Laframboise Point that here define the negative ε_{pyr} excursion (Fig. 2).

As such, it seems most parsimonious to correlate the Laframboise Point data with a well-ventilated and oxic glacial ocean. If anything, increased oxygen availability in deep waters is likely to have resulted in a corresponding increase in the abundance and activity of sulfur disproportionating organisms at the time of the $\delta^{34}S$ excursion. Such an increase in disproportionation would be expected to lead to an increase in ε_{pyr}, rather than the observed decrease. On the other hand, reduced fractionations and heavy $\delta^{34}S_{pyr}$ values are often observed in physically reworked shallow marine sediments that have undergone extensive oxidative and reductive sulfur cycling (Aller et al., 2010). Variations within the oxidative sulfur cycle, especially in the context of enhanced sediment reworking during glacioeustatic sea level fall, remain a plausible explanation for the observed ε_{pyr} behavior and require further investigation.

Although the above argument focuses on the relationship of the Anticosti $\delta^{34}S_{pyr}$ and climate records to those from South China and Denmark, sequence stratigraphic and biostratigraphic work correlate the Laframboise Point section with the end of the Hirnantian rather than the entire Hirnantian (Desrochers et al., 2010; Achab et al., 2011). In this scenario, the Laframboise Point data may correspond to upper Hirnantian strata deposited in a largely anoxic ocean, in which case the shut down of the oxidative

sulfur cycle might be able to explain the negative ε_{pyr} excursion. Two factors, however, make this interpretation unlikely. First, the $\delta^{34}S_{pyr}$ excursion is in the lower Hirnantian in Denmark, Scotland, and two of the three sections in South China (see compilation in Hammarlund et al. (2012)). Second, none of the redox proxies indicating anoxia in the upper Hirnantian return to oxic conditions in the lower Silurian (Hammarlund et al., 2012; Yan et al., 2012). A return to oxic conditions would be required in order to reintroduce oxidative sulfur cycling and end the observed ε_{pyr} excursion. Although we do not consider it likely for reasons outlined above, we cannot exclude the possibility that expanded anoxia drove the changes in ε_{pyr} we observe at Laframboise Point due to a temporary shut down of the oxidative portion of the sulfur cycle. Future studies focusing on minor sulfur isotopes may have the potential to unravel changes in the relative proportions of sulfur disproportionation, oxidation, and reduction during the Hirnantian (e.g., Farquhar et al., 2003; Johnston et al., 2005a, 2005b).

5.4.3. Diffusion-limited sulfate exchange in early diagenetic pore fluids

Yan et al. (2009) interpreted the Hirnantian $\delta^{34}S_{pyr}$ excursion to record a transitory change to more oxic conditions that forced the chemocline deeper into the sediments. This resulted in limited porewater exchange with the overlying water column and a gradual enrichment of porewater $\delta^{34}S_{SO_4}$ and $\delta^{34}S_{pyr}$ as the result of ongoing sedimentary pyrite formation. Even though porewater sulfate may be isotopically enriched in this scenario, any incorporation into diagenetic carbonates is believed to be a quantitatively insignificant component to the overall $\delta^{34}S_{CAS}$ signature (Lyons et al., 2004). In such a scenario, the pools of sulfur sampled by sedimentary pyrite (porewater sulfate) and carbonate associated sulfate (overlying water column) are distinct (Lyons et al., 2004), allowing for their isotopic systematics to evolve independently. Therefore, an apparent decrease in ε_{pyr} could reflect chemocline migration that resulted in distinct reservoirs contributing to the oxidized (water column) and reduced (pore water) sulfur species in Hirnantian strata, rather than any change in the biological fractionation itself.

This mechanism is consistent with our paired $\delta^{34}S$ data from Laframboise Point, and we cannot rule it out. However, it is not clear how a change in the chemocline depth would be coupled to the carbon cycle in such a way as to produce the observed anti-correlated changes in $\delta^{13}C_{carb}$ and ε_{pyr} (Fig. 3). Rather, a change in chemocline depth is more likely to be tightly coupled to changes in the redox state of the overlying ocean, and therefore perhaps to changes in ocean stratification or overturn or glacio-eustatic sea level changes. Although clumped isotope data indicate that the glacial *maximum* corresponds to the strata hosting the ε_{pyr} excursion, they also indicate the presence of continental ice in the pre-Hirnantian Katian and post-Hirnantian Rhuddanian stages (Finnegan et al., 2011). If a strong equator to pole thermal gradient stimulated ocean overturn and ventilation (Herrmann et al., 2004), we might expect the ε_{pyr} excursion to coincide with the duration of continental ice cover rather than the $\delta^{13}C_{carb}$ excursion.

5.4.4. MSR rate

It has long been recognized that sulfate reduction rates can influence isotopic fractionation (e.g., Kaplan and Rittenberg, 1964; Chambers et al., 1975). Recent work has highlighted the dependence of isotopic fractionation during MSR on cell-specific sulfate reduction rates (csSRR) (Habicht and Canfield, 2001; Canfield, 2001b; Canfield et al., 2006; Sim et al., 2011a, 2011b). Here, high metabolic rates result in minimal isotopic fractionation, whereas low rates allow for larger fractionations to be expressed; this can produce substantial variation in ε_{pyr} with values from ~0‰ to ~70‰ (e.g., Sim et al., 2011a, 2011b). The quantitative framework that has emerged from these experiments provides a tool for assessing sulfur isotope records in deep time. Environmental changes that affect csSRR could therefore plausibly cause changes in ε_{pyr} that are recorded in the sulfur isotope record. For example, John et al. (2010) invoked enhanced SRR rates due to either changing microbial assemblages or increased delivery of organic matter to the seafloor to explain apparent decreases in ε_{pyr} (steady $\delta^{34}S_{CAS}$ paired with increasing $\delta^{34}S_{pyr}$) during the Late Devonian. While other possibilities may exist for varying ε_{pyr}, the Hirnantian $\delta^{34}S_{pyr}$ excursion could be explained by an increase in csSRR during the Hirnantian. Given that Hirnantian strata were deposited in a world undergoing substantial environmental change, it is perhaps not surprising that biological fractionation during sulfur cycling may have varied.

5.5. Hirnantian glaciation, microbial sulfur cycling, and C–S coupling

How then can we reconcile increased MSR rates inferred from the sulfur isotope record with environmental change accompanying the Hirnantian glaciation? We seek a set of processes that would yield the statistically significant inverse correlation between ε_{pyr} and $\delta^{13}C_{carb}$ (Fig. 3) in the larger context of the Hirnantian glacial maximum. Broadly, we propose that Hirnantian glaciation and cooling led to increased availability of organic substrates in marine sediments, which in turn increased csSRR and led to the transient decrease in ε_{pyr}. There are at least two mechanisms we are aware of linking glacial conditions and/or cold ocean temperatures to enhanced burial of organic matter. First, primary productivity may spike from synglacial upwelling of nutrients (Berry and Wilde, 1978; Brenchley et al., 1994). This hypothesis is supported by satellite observations of the modern global ocean showing a tight correlation between net primary productivity and temperature; a higher nutrient flux during cooler years is attributed to increased mixing of surface and deep waters as tropical and mid-latitude ocean stratification weakens (Behrenfeld et al., 2006). Secondly, colder temperatures lead to reduced organic remineralization rates (Hargrave, 1969; Thamdrup et al., 1998; Stanley, 2010; Finnegan et al., 2012a). These mechanisms (one focused on enhanced production of organic matter and the other on enhanced preservation) are not mutually exclusive and both processes are compatible with the hypothesis considered here.

The "productivity hypothesis" for the origin of the Hirnantian glaciation and $\delta^{13}C$ excursion posits that invigorated overturning ocean circulation delivered nutrients from the deep ocean to the surface, stimulating primary productivity (Brenchley et al., 1994, 1995). This productivity increase drew down atmospheric pCO_2 levels, increased f_{org}, and led to both glaciation and the positive $\delta^{13}C$ excursion. The synchronicity of maximum ice build up with the peak of the $\delta^{13}C$ excursion is supported by clumped isotope paleothermometry data from Anticosti Island (Finnegan et al., 2011). Increased burial flux of organic matter due to elevated productivity would have resulted in a greater abundance of organic substrates in marine sediments.

An alternate interpretation for the coincidence of cooling ocean temperatures and the positive $\delta^{13}C$ excursion highlights the temperature dependence of organic remineralization rates (Hargrave, 1969; Thamdrup et al., 1998; Stanley, 2010; Finnegan et al., 2012a). Chemical reaction rates slow with decreasing temperature, as predicted by the Arrhenius equation and quantified by the Q10 parameter (Stanley, 2010; Finnegan et al., 2012a). We hypothesize that maximum glacial conditions and the associated minimum in global ocean temperatures during the Hirnantian may have acted to enhance the preservation potential of organic matter in sediments through decreased aerobic

respiration rates in the water column. This would have led to an effective increase in the organic burial flux, increasing f_{org} and driving the positive $\delta^{13}C$ excursion. Importantly, this mechanism is independent of any changes in ocean circulation or enhanced nutrient delivery to the surface ocean, processes for which there is little unambiguous and direct geological evidence. However, these mechanisms (increased productivity and decreased remineralization) are not mutually exclusive and both may have contributed to an increase in organic substrates available for MSR during Hirnantian time.

The increased availability of labile organic substrates for sulfate reduction would be expected to increase MSR rates and thereby decrease ε_{pyr} (Sim et al., 2011a, 2011b), providing a positive $\delta^{34}S_{pyr}$ excursion synchronous with the $\delta^{13}C$ enrichment (Yan et al., 2009; Zhang et al., 2009; Gorjan et al., 2012; Hammarlund et al., 2012). Thus, increased organic carbon availability and correspondingly enhanced rates of MSR provide a plausible explanation for the co-occurrence of the synchronous ε_{pyr} and $\delta^{13}C$ excursions during the Hirnantian glacial maximum (Figs. 2 and 3). If the greater abundance of organic substrates for sulfate reduction was due to cold temperatures slowing the metabolic rates of aerobic heterotrophs, it is reasonable to question whether the decreased temperatures affected sulfate reducers in the same way; this could potentially counteract the increase in MSR rates brought on by the enhanced availability of organic substrates. However, given the nonlinear temperature dependence of metabolic activity (e.g., Stanley, 2010), aerobic respiration in (presumably warmer) surface waters is likely to have been more impacted by temperature change than sulfate reducing organisms in pore waters. Even if aerobic respiration and MSR were equally slowed by a temperature change, the high efficiency of aerobic respiration is such that a small decrease in respiration rates would result in substantial increase in organic delivery to the sediments. Furthermore, ε_{pyr} during MSR is affected by the lability of the organic substrate as well as by its abundance (Sim et al., 2011b). As temperatures fall and aerobic respiration rates decline, more highly labile organic matter escapes aerobic decomposition and becomes available to MSR communities in the sediment. Because sulfate reducers impart a lower isotope fractionation when metabolizing more labile substrates (Sim et al., 2011b), the changing nature of the electron donors escaping aerobic respiration may have also been an important factor in reducing ε_{pyr} during the glacial maximum.

Increased MSR rates may have led to increased sulfide production and eventually pyrite burial (pending iron availability). Indeed, organic carbon and pyrite burial are often thought to vary sympathetically in normal marine environments (Raiswell and Berner, 1986; Lin and Morse, 1991). However, the magnitude of change in f_{pyr}, associated with a corresponding change in f_{org} sufficient to drive a 4‰ $\delta^{13}C$ excursion, would be insufficient to detect in the sulfur isotopic record during Hirnantian time, as discussed in Section 5.3.1. *Therefore, although pyrite burial may have increased when organic availability and MSR rates were elevated, it could not have driven the $\delta^{34}S_{pyr}$ excursion.* Rather, we view the $\delta^{34}S_{pyr}$ excursion as the result of a decrease in ε_{pyr} driven by enhanced csSRR.

Finally, we note that the sulfur isotope data from Anticosti Island do not directly address the "weathering hypothesis," which invokes synglacial changes in $\delta^{13}C_{in}$ as the driver for the Hirnantian $\delta^{13}C$ excursion (Kump et al., 1999; Melchin and Holmden, 2006). An analogous origin for the end Hirnantian $\delta^{34}S_{pyr}$ excursion through changes in $\delta^{34}S_{in}$ is precluded based both on the duration of the Hirnantian excursion and the absence of a parallel excursion in $\delta^{34}S_{CAS}$ (unlike the parallel excursions in $\delta^{13}C_{carb}$ and $\delta^{13}C_{org}$) (Section 5.3.1). However, to the degree that a change in weathering regime could be responsible for driving the observed changes in ε_{pyr} (e.g., through differential nutrient delivery driving enhanced biological productivity), the weathering hypothesis may still hold explanatory power for understanding variations in Hirnantian biogeochemical cycling.

5.6. Differential response times of C and S cycle perturbations

The differential temporal evolution of the paired carbon and sulfur isotopic data shown in Fig. 5 is useful in highlighting new methods for constraining environment perturbations to biogeochemical cycles. Specifically, the relative timing of the isotopic responses to a synchronous change in organic carbon and pyrite burial can provide constraints on the relative sizes of the reservoirs of marine carbon and sulfur, respectively. It can be seen from Fig. 5 that the peaks of the excursion in $\delta^{34}S_{SO_4}$ and $\delta^{34}S_{pyr}$ experience a time lag relative to the carbon isotope excursions. This is a result of the different response times (τ, the ratio of reservoir size to input and output fluxes) of the carbon and sulfur biogeochemical cycles. Thus, although at first glance it appears somewhat counterintuitive, it is *the differential stratigraphic expression of carbon and sulfur isotopic excursions that should be the hallmark of a single environmental perturbation that affected organic carbon and pyrite burial in parallel*. In addition, in such a case, the temporal lag between $\delta^{13}C$ and $\delta^{34}S$ extrema would provide a direct measurement of the relative response times of the two systems and could, for example, provide new constraints on the temporal evolution of marine sulfate and/or dissolved inorganic carbon reservoirs over Earth history.

Finally, we note that if changes in ε_{pyr} were responsible for the $\delta^{34}S_{pyr}$ excursion, the lack of a corresponding *negative* excursion in $\delta^{34}S_{CAS}$ places constraints on the residence time of sulfate within the oceans and therefore on the size of the marine sulfate reservoir during the Hirnantian Stage. For short residence times, a parallel, negative excursion in $\delta^{34}S_{CAS}$ would be visible during a transient decrease in ε_{pyr} (e.g., Fig. 6). The absence of any detectable (greater than the ~5‰ scatter in our data) negative excursion in $\delta^{34}S_{CAS}$ (Fig. 2) suggests that seawater sulfate concentrations during the Hirnantian State were not less than ~5 mM (and possibly substantially higher), in agreement with independent results from fluid inclusion analysis (e.g., Brennan and Lowenstein, 2002; Lowenstein et al., 2003).

6. Conclusions

Our modeling and paired $\delta^{34}S_{pyr}$–$\delta^{34}S_{CAS}$ data provide new insights into the origin of the Hirnantian $\delta^{34}S_{pyr}$ excursion and the coupling between the carbon and sulfur cycles during this interval of environmental change. An increase in f_{pyr} is not consistent with the timescale of the excursion, nor is it consistent with the absence of a parallel excursion in $\delta^{34}S_{CAS}$ from Laframboise Point. Therefore models of Hirnantian ocean redox changes based on changes in f_{pyr} and the role of anoxia in the end Ordovician mass extinction may need to be reevaluated. We show that a time-varying biological fractionation ε_{pyr} is a plausible mechanism capable of generating the observed 20‰ global $\delta^{34}S_{pyr}$ enrichment in Hirnantian strata within the constrained timescale and without yielding a parallel excursion in seawater sulfate isotope ratios ($\delta^{34}S_{SO_4}$). The decrease in ε_{pyr} may have been caused by increasing cell-specific sulfate reduction rates (which are sensitive to the abundance, type, and lability of metabolically relevant substrates), although changes in the depth of the chemocline and resulting porewater sulfate exchange cannot be ruled out. A change in ε_{pyr} provides a clear mechanism to explain the parallel excursions in $\delta^{13}C$ and $\delta^{34}S_{pyr}$ (enhanced availability of organic substrates driving enhanced sulfate reduction rates). The presence of the $\delta^{34}S$ excursion in pyrite but not coeval sulfate can be

ascribed to differential biological activity within a dynamic sulfur cycle, *a signature that is neither transmitted through nor preserved in the parent marine sulfate reservoir*. Such dynamic models may improve our understanding of the differential occurrence and magnitude of isotopic signatures over Earth history as preserved in reservoir proxies ($\delta^{13}C_{carb}$ and $\delta^{34}S_{SO_4}$) vs. those filtered by biological fractionation ($\delta^{13}C_{org}$ and $\delta^{34}S_{pyr}$, respectively).

Acknowledgments

This research as supported by a grant from the Agouron Institute, a Packard Fellowship, and a Hansewissenschaftskolleg Fellowship to DAF. DSJ gratefully acknowledges support from Amherst College. We thank Woody Fischer and Seth Finnegan for valuable discussions. We thank Associate Editor Gideon Henderson and an anonymous reviewer for helpful comments. Dwight McCay and Claire Beaudoin assisted with sample preparation and analysis at Washington University.

Appendix A. Supporting information

Supplementary data associated with this article can be found in the online version at http://dx.doi.org/10.1016/j.epsl.2012.12.015.

References

Achab, A., Asselin, E., Desrochers, A., Riva, J.F., Farley, C., 2011. Chitinozoan biostratigraphy of a new Upper Ordovician stratigraphic framework for Anticosti Island, Canada. Geol. Soc. Am. Bull. 123, 186–205.

Aller, R.C., Madrid, V., Chistoserdov, A., Aller, J.Y., Heilbrun, C., 2010. Unsteady diagenetic processes and sulfur biogeochemistry in tropical deltaic muds: implications for oceanic isotope cycles and the sedimentary record. Geochim. Cosmochim. Acta 74, 4671–4692.

Banner, J.L., Hanson, G.N., 1990. Calculation of simultaneous isotopic and trace element variations during water–rock interaction with applications to carbonate diagenesis. Geochim. Cosmochim. Acta 54, 3123–3137.

Behrenfeld, M.J., O'Malley, R.T., Siegel, D.A., McClain, C.R., Sarmiento, J.L., Feldman, G.C., Milligan, A.J., Falkowski, P.G., Letelier, R.M., Boss, E.S., 2006. Climate-driven trends in contemporary ocean productivity. Nature 444, 752–755.

Berry, W.B.N., Wilde, P., 1978. Progressive ventilation of the oceans; an explanation for the distribution of the lower Paleozoic black shales. Am. J. Sci. 278, 257.

Berry, W.B.N., Wilde, P., Quinby-Hunt, M.S., 1990. Late Ordovician graptolite mass mortality and subsequent early Silurian re-radiation. In: Kauffman, E.G., Walliser, O.H. (Eds.), Extinction Events in Earth History. pp. 115–123.

Brand, U., Veizer, J., 1980. Chemical diagenesis of a multicomponent carbonate system-1: Trace elements. J. Sediment. Petrol. 50, 1219–1236.

Brenchley, P.J., Carden, G.A.F., Hints, L., Kaljo, D., Marshall, J.D., Martma, T., Meidla, T., Nolvak, J., 2003. High-resolution stable isotope stratigraphy of Upper Ordovician sequences: constraints on the timing of bioevents and environmental changes associated with mass extinction and glaciation. Geol. Soc. Am. Bull. 115, 89–104.

Brenchley, P.J., Carden, G.A.F., Marshall, J.D., 1995. Environmental changes associated with the "first strike" of the Late Ordovician mass extinction. Mod. Geol. 20, 69–82.

Brenchley, P.J., Marshall, J.D., 1999. Relative timing and critical events during the late Ordovician mass extinction—new data from Oslo. Acta Univ. Carolinae—Geol. 43, 187–190.

Brenchley, P.J., Marshall, J.D., Carden, G.A.F., Robertson, D., Long, D.G.F., Meidla, T., Hints, L., Anderson, T.F., 1994. Bathymetric and isotopic evidence for a short-lived Late Ordovician glaciation in a greenhouse period. Geology 22, 295–298.

Brennan, S.T., Lowenstein, T.K., 2002. The major-ion composition of Silurian seawater. Geochim. Cosmochim. Acta 66, 2683–2700.

Burdett, J.W., Arthur, M.A., Richardson, M., 1989. A Neogene seawater sulfate isotope age curve from calcareous pelagic microfossils. Earth Planet. Sci.Lett 94, 189–198.

Burton, E.D., Sullivan, L.A., Bush, R.T., Johnston, S.G., Keene, A.F., 2008. A simple and inexpensive chromium-reducible sulfur method for acid-sulfate soils. Appl. Geochem 23, 2759–2766.

Canfield, D.E., 2001a. Biogeochemistry of Sulfur Isotopes. Rev. Mineral. Geochem., 607–636.

Canfield, D.E., 2001b. Isotope fractionation by natural populations of sulfate-reducing bacteria. Geochim. Cosmochim. Acta 65, 1117–1124.

Canfield, D.E., 2004. The evolution of the Earth surface sulfur reservoir. Am. J. Sci. 304, 839–861.

Canfield, D.E., Farquhar, J., Zerkle, A.L., 2010. High isotope fractionations during sulfate reduction in a low-sulfate euxinic ocean analog. Geology 38, 415–418.

Canfield, D.E., Olesen, C.A., Cox, R.P., 2006. Temperature and its control of isotope fractionation by a sulfate-reducing bacterium. Geochim. Cosmochim. Acta 70, 548–561.

Canfield, D.E., Teske, A., 1996. Late Proterozoic rise in atmospheric oxygen concentration inferred from phylogenetic and sulphur-isotope studies. Nature 382, 127–132.

Canfield, D.E., Thamdrup, B., Fleischer, S., 1998. Isotope fractionation and sulfur metabolism by pure and enrichment cultures of elemental sulfur-disproportionating bacteria. Limnol. Oceanogr. 43, 253–264.

Chambers, L.A., Trudinger, P.A., Burns, M.S., Smith, J.W., 1975. Fractionation of sulfur isotopes by continuous cultures of *Desulfovibrio desulfuricans*. Can. J. Microbiol. 21, 1602–1607.

Copper, P., 1999. Brachiopods during and after the Late Ordovician mass extinctions, Anticosti Island, E Canada. Acta Univ. Carolinae—Geol. 43, 207–209.

Delabroye, A., Munnecke, A., Vecoli, M., Copper, P., Tribovillard, N., Joachimski, M.M., Desrochers, A., Servais, T., 2011. Phytoplankton dynamics across the Ordovician/Silurian boundary at low palaeolatitudes: correlations with carbon isotopic and glacial events. Palaeogeogr. Palaeoclim. Palaeoecol. 312, 79–97.

Delabroye, A., Vecoli, M., 2010. The end-Ordovician glaciation and the Hirnantian Stage: a global review and questions about Late Ordovician event stratigraphy. Earth Sci. Rev. 98, 269–282.

Desrochers, A., Farley, C., Achab, A., Asselin, E., 2010. A far-field record of the end Ordovician glaciation: the Ellis Bay Formation, Anticosti Island, Eastern Canada. Palaeogeogr. Palaeoclim. Palaeoecol. 296, 248–263.

Farquhar, J., Johnston, D.T., Wing, B.A., Habicht, K.S., Canfield, D.E., Airieau, S., Thiemens, M.H., 2003. Multiple sulphur isotopic interpretations of biosynthetic pathways: implications for biological signatures in the sulphur isotope record. Geobiology 1, 27–36.

Fike, D.A., Grotzinger, J.P., 2008. A paired sulfate–pyrite $\delta^{34}S$ approach to understanding the evolution of the Ediacaran–Cambrian sulfur cycle. Geochim. Cosmochim. Acta 72, 2636–2648.

Fike, D.A., Grotzinger, J.P., Pratt, L.M., Summons, R.E., 2006. Oxidation of the Ediacaran ocean. Nature 444, 744–747.

Finnegan, S., Bergmann, K., Eiler, J., Jones, D.S., Fike, D.A., Eisenman, I., Hughes, N., Tripati, A., Fischer, W.W., 2011. The magnitude and duration of Late Ordovician–Early Silurian glaciation. Science 331, 903–906.

Finnegan, S., Fike, D.A., Jones, D.S., Fischer, W.W., 2012a. A temperature-dependent positive feedback on the magnitude of carbon isotope excursions. Geosci. Can. 139, 122–131.

Finnegan, S., Heim, N.A., Peters, S.E., Fischer, W.W., 2012b. Climate change and the selective signature of the Late Ordovician mass extinction. Proc. Natl. Acad. Sci. 109, 6829–6834.

Ghienne, J.-F., 2003. Late Ordovician sedimentary environments, glacial cycles, and post-glacial transgression in the Taoudeni Basin, West Africa. Palaeogeogr. Palaeoclim. Palaeoecol. 189, 117–145.

Ghosh, P., Adkins, J., Affek, H., Balta, B., Guo, W., Schauble, E., Schrag, D.P., Eiler, J.M., 2006. 13C–18O bonds in carbonate minerals: a new kind of paleothermometer. Geochim. Cosmochim. Acta 70, 1439–1456.

Gill, B.C., Lyons, T.W., Frank, T.D., 2008. Behavior of carbonate-associated sulfate during meteoric diagenesis and implications for the sulfur isotope paleoproxy. Geochim. Cosmochim. Acta 72, 4699–4711.

Gill, B.C., Lyons, T.W., Young, S.A., Kump, L.R., Knoll, A.H., Saltzman, M.R., 2011. Geochemical evidence for widespread euxinia in the Later Cambrian ocean. Nature 469, 80–83.

Given, R.K., Lohmann, K., 1986. Isotopic evidence for the early meteoric diagenesis of the reef facies, Permian Reef Complex of West Texas and New Mexico. J. Sediment. Petrol. 56, 183–193.

Gorjan, P., Kaiho, K., Fike, D.A., Xu, C., 2012. Carbon- and sulfur-isotope geochemistry of the Hirnantian (Late Ordovician) Wangjiawan (Riverside) section, South China: global correlation and environmental event interpretation. Palaeogeogr. Palaeoclim. Palaeoecol. 337–338, 14–22.

Habicht, K.S., Canfield, D.E., 1997. Sulfur isotope fractionation during bacterial sulfate reduction in organic-rich sediments. Geochim. Cosmochim. Acta 61, 5351–5361.

Habicht, K.S., Canfield, D.E., 2001. Isotope fractionation by sulfate-reducing natural populations and the isotopic composition of sulfide in marine sediments. Geology 29, 555–558.

Habicht, K.S., Canfield, D.E., Rethmeier, J., 1998. Sulfur isotope fractionation during bacterial reduction and disproportionation of thiosulfate and sulfite. Geochim. Cosmochim. Acta 62, 2585–2595.

Habicht, K.S., Gade, M., Thamdrup, B., Berg, P., Canfield, D.E., 2002. Calibration of sulfate levels in the Archean Ocean. Science 298, 2372–2374.

Halevy, I., Peters, S.E., Fischer, W.W., 2012. Sulfate burial constraints on the Phanerozoic sulfur cycle. Science 337, 331–334.

Hammarlund, E.U., Dahl, T.W., Harper, D.A.T., Bond, D.P.G., Nielsen, A.T., Bjerrum, C.J., Schovsbo, N.H., Schönlaub, H.P., Zalasiewicz, J.A., Canfield, D.E., 2012. A sulfidic driver for the end-Ordovician mass extinction. Earth Planet. Sci. Lett. 331–332, 128–139.

Hargrave, B.T., 1969. Similarity of oxygen uptake by benthic communities. Limnol. Oceanogr. 14, 801–805.

Hayes, J.M., Strauss, H., Kaufman, A.J., 1999. The abundance of ^{13}C in marine organic matter and isotopic fractionation in the global biogeochemical cycle of carbon during the past 800 Ma. Chem. Geol. 161, 103–125.

Herrmann, A.D., Haupt, B., Patzkowsky, M., Seidov, D., Slingerland, R.L., 2004. Response of Late Ordovician paleoceanography to changes in sea level, continental drift, and atmospheric pCO_2: potential causes for long-term cooling and glaciation. Palaeogeogr. Palaeoclim. Palaeoecol. 210, 385–401.

Hints, L., Hints, O., Kaljo, D., Kiipli, T., Männik, P., Nolvak, J., Paernaste, H., 2010. Hirnantian (latest Ordovician) bio- and chemostratigraphy of the Stirnas-18 core, western Latvia. Est. J. Earth Sci. 59, 1–24.

Hurtgen, M.T., Pruss, S.B., Knoll, A.H., 2009. Evaluating the relationship between the carbon and sulfur cycles in the later Cambrian ocean: an example from the Port au Port Group, western Newfoundland, Canada. Earth Planet. Sci. Lett. 281, 288–297.

John, E.H., Wignall, P.B., Newton, R.J., Bottrell, S.H., 2010. $\delta^{34}S_{CAS}$ and $\delta^{18}O_{CAS}$ records during the Frasnian–Famennian (Late Devonian) transition and their bearing on mass extinction models. Chem. Geol. 275, 221–234.

Johnston, D.T., Farquhar, J., Wing, B.A., Kaufman, A.J., Canfield, D.E., Habicht, K.S., 2005a. Multiple sulfur isotope fractionations in biological systems: a case study with sulfate reducers and sulfur disproportionators. Am. J. Sci. 305, 645–660.

Johnston, D.T., Wing, B.A., Farquhar, J., Kaufman, A.J., Strauss, H., Lyons, T.W., Kah, L.C., Canfield, D.E., 2005b. Active microbial sulfur disproportionation in the Mesoproterozoic. Science 310, 1477–1479.

Jones, D.S., Fike, D.A., Finnegan, S., Fischer, W.W., Schrag, D.P., McCay, D., 2011. Terminal Ordovician carbon isotope stratigraphy and glacioeustatic sea-level change across Anticosti Island (Quebec, Canada). Geol. Soc. Am. Bull. 123, 1645–1664.

Kah, L.C., Lyons, T.W., Frank, T.D., 2004. Low marine sulphate and protracted oxygenation of the proterozoic biosphere. Nature 431, 834–838.

Kaljo, D., Hints, L., Maennik, P., Nolvak, J., 2008. The succession of Hirnantian events based on data from Baltica: brachiopods, chitinozoans, conodonts, and carbon isotopes. Est. J. Earth Sci. 57, 197–218.

Kaljo, D., Hints, L., Martma, T., Nolvak, J., Oraspőld, A., 2004. Late Ordovician carbon isotope trend in Estonia, its significance in stratigraphy and environmental analysis. Palaeogeogr. Palaeoclim. Palaeoecol. 210, 165–185.

Kampschulte, A., Strauss, H., 2004. The sulfur isotopic evolution of Phanerozoic seawater based on the analysis of structurally substituted sulfate in carbonates. Chem. Geol. 204, 255–286.

Kaplan, I., Rittenberg, S., 1964. Microbiological fractionation of sulphur isotopes. J. Gen. Microbiol. 34, 195.

Kaufman, A.J., Hayes, J., Knoll, A.H., Germs, G., 1991. Isotopic compositions of carbonates and organic carbon from upper Proterozoic successions in Namibia: stratigraphic variation and the effects of diagenesis and metamorphism. Precambrian Res. 49, 301–327.

Kump, L.R., Arthur, M.A., Patzkowsky, M., Gibbs, M., Pinkus, D.S., Sheehan, P.M., 1999. A weathering hypothesis for glaciation at high atmospheric pCO_2 during the Late Ordovician. Palaeogeogr. Palaeoclim. Palaeoecol. 152, 173–187.

Le Heron, D., Dowdeswell, J., 2009. Calculating ice volumes and ice flux to constrain the dimensions of a 440 Ma North African ice sheet. J. Geol. Soc. London 166, 277–281.

Lin, S., Morse, J.W., 1991. Sulfate reduction and iron sulfide mineral formation in Gulf of Mexico anoxic sediments. Am. J. Sci. 291, 55–89.

Long, D.G.F., 1993. Oxygen and carbon isotopes and event stratigraphy near the Ordovician–Silurian boundary, Anticosti Island Quebec. Palaeogeogr. Palaeoclim. Palaeoecol. 104, 49–59.

Long, D.G.F., 2007. Tempestite frequency curves: a key to Late Ordovician and Early Silurian subsidence, sea-level change, and orbital forcing in the Anticosti foreland basin, Quebec, Canada. Can. J. Earth Sci. 44, 413–431.

Long, D.G.F., Copper, P., 1987. Late Ordovician sand-wave complexes on Anticosti Island, Quebec: a marine tidal embayment? Can. J. Earth Sc. 24, 1821–1832.

Lowenstein, T.K., Hardie, L.A., Timofeeff, M.N., Demicco, R.V., 2003. Secular variation in seawater chemistry and the origin of calcium chloride basinal brines. Geology 31, 857.

Loyd, S.J., Marenco, P.J., Hagadorn, J.W., Lyons, T.W., Kaufman, A.J., Sour-Tovar, F., Corsetti, F.A., 2012. Sustained low marine sulfate concentrations from the Neoproterozoic to the Cambrian Insights from carbonates of northwestern Mexico and eastern California. Earth Planet. Sci. Lett. 339–340, 79–94.

Lyons, T.W., Walter, L., Gellatly, A., Martini, A., Blake, R., 2004. Sites of anomalous organic remineralization in the carbonate sediments of South Florida, USA: the sulfur cycle and carbonate-associated sulfate. In: Amend, J.P., Edwards, K.J., Lyons, T.W. (Eds.), Sulfur Biogeochemistry—Past and Present. Geological Society of America, Boulder, CO, pp. 161–176.

Marenco, P.J., Corsetti, F.A., Hammond, D.E., Kaufman, A.J., 2008a. Oxidation of pyrite during extraction of carbonate associated sulfate. Chem. Geol. 247, 124–132.

Marenco, P.J., Corsetti, F.A., Kaufman, A.J., Bottjer, D.J., 2008b. Environmental and diagenetic variations in carbonate associated sulfate: an investigation of CAS in the Lower Triassic of the western USA. Geochim. Cosmochim. Acta 72, 1570–1582.

Melchin, M.J., 2008. Restudy of some Ordovician–Silurian boundary graptolites from Anticosti Island, Canada, and their biostratigraphic significance. Lethaia 41, 155–162.

Melchin, M.J., Holmden, C.E., 2006. Carbon isotope chemostratigraphy in Arctic Canada: sea-level forcing of carbonate platform weathering and implications for Hirnantian global correlation. Palaeogeogr. Palaeoclim. Palaeoecol. 234, 186–200.

Parnell, J., Boyce, A.J., Mark, D., Bowden, S., Spinks, S., 2010. Early oxygenation of the terrestrial environment during the Mesoproterozoic. Nature 468, 290–293.

Petryk, A.A., 1981. Stratigraphy, sedimentology and paleogeography of the Upper Ordovician–Lower Silurian of Anticosti Island, Quebec. In: Lesperance, P.J. (Ed.), Field Meeting: Anticosti-Gaspe, Quebec. International Union of Geological Sciences, pp. 11–39.

Pope, M.C., Steffen, J.B., 2003. Widespread, prolonged late Middle to Late Ordovician upwelling in North America: a proxy record of glaciation? Geology 31, 63–66.

Poussart, P.F., Weaver, A., Barnes, C.R., 1999. Late Ordovician glaciation under high atmospheric CO_2: a coupled model analysis. Paleoceanography 14, 542–558.

Raiswell, R., Berner, R.A., 1986. Pyrite and organic matter in Phanerozoic normal marine shales. Geochim. Cosmochim. Acta 50, 1967–1976.

Riva, J.F., 1988. Graptolites at and below the Ordovician–Silurian boundary on Anticosti Island, Canada. Bull. Br. Mus. Nat. Hist. (Geol.) 43, 221–237.

Sadler, P.M., Cooper, R.A., Melchin, M., 2009. High-resolution, early Paleozoic (Ordovician–Silurian) time scales. Geol. Soc. Am. Bull. 121, 887–906.

Sami, T., Desrochers, A., 1992. Episodic sedimentation on an Early Silurian, storm-dominated carbonate ramp, Becscie and Merrimack formations, Anticosti Island, Canada. Sedimentology 39, 355–381.

Sheehan, P.M., 2001. The Late Ordovician mass extinction. Annu. Rev. Earth Planet. Sci. 29, 331–364.

Sim, M.S., Bosak, T., Ono, S., 2011a. Large sulfur isotope fractionation does not require disproportionation. Science 333, 74–77.

Sim, M.S., Ono, S., Donovan, K., Templer, S.P., Bosak, T., 2011b. Effect of electron donors on the fractionation of sulfur isotopes by a marine *Desulfovibrio* sp. Geochim. Cosmochim. Acta 75, 4244–4259.

Stanley, S.M., 2010. Relation of Phanerozoic stable isotope excursions to climate, bacterial metabolism, and major extinctions. Proc. Natl. Acad. Sci. 107, 19185–19189.

Sutcliffe, O., Dowdeswell, J., Whittington, R., Theron, J.N., Craig, J., 2000. Calibrating the Late Ordovician glaciation and mass extinction by the eccentricity cycles of Earth's orbit. Geology 28, 967–970.

Thamdrup, B., Hansen, J.W., Jørgensen, B.B., 1998. Temperature dependence of aerobic respiration in a coastal sediment. FEMS Microbiol. Ecol. 25, 189–200.

Underwood, C.J., Crowley, S., Marshall, J.D., Brenchley, P.J., 1997. High-resolution carbon isotope stratigraphy of the basal Silurian Stratotype (Dob's Linn, Scotland) and its global correlation. J. Geol. Soc. London 154, 709–718.

Vaslet, D., 1990. Upper Ordovician glacial deposits in Saudi Arabia. Episodes 13, 147–161.

Veizer, J., 1983. Chemical diagenesis of carbonates: theory and application of trace element technique. In: Arthur, M.A., Anderson, T.F., Kaplan, I.R., Veizer, J., Land, L. (Eds.), Stable Isotopes in Sedimentary Geology. Society of Economic Paleontologists and Mineralogists, pp. 1–100.

Waldron, J.W.F., Anderson, S., Cawood, P., Goodwin, L., Hall, J., Jamieson, R., Palmer, S., Stockmal, G.S., Williams, P., 1998. Evolution of the Appalachian Laurentian margin: lithoprobe results in western Newfoundland. Can. J. Earth Sci. 35, 1271–1287.

Wang, K., Orth, C.J., Attrep Jr, M., Chatterton, B.D.E., Wang, X., Li, J.-J., 1993. The great latest Ordovician extinction on the South China Plate: chemostratigraphic studies of the Ordovician–Silurian boundary interval on the Yangtze Platform. Palaeogeogr. Palaeoclim. Palaeoecol. 104, 61–79.

Wilde, P., Quinby-Hunt, M.S., Berry, W.B.N., 1990. Vertical advection from oxic or anoxic water from the main pycnocline as a cause of rapid extinction or rapid radiations. In: Kauffman, E.G., Walliser, O.H. (Eds.), Extinction Events in Earth History. pp. 85–98.

Wortmann, U.G., Chernyavsky, B.M., 2007. Effect of evaporite deposition on Early Cretaceous carbon and sulphur cycling. Nature 446, 654–656.

Wortmann, U.G., Paytan, A., 2012. Rapid variability of seawater chemistry over the past 130 million years. Science 337, 334–336.

Yan, D., Chen, D., Wang, Q., Wang, J., 2012. Predominance of stratified anoxic Yangtze Sea interrupted by short-term oxygenation during the Ordo-Silurian transition. Chem. Geol. 291, 69–78.

Yan, D., Chen, D., Wang, Q., Wang, J., Wang, Z., 2009. Carbon and sulfur isotopic anomalies across the Ordovician–Silurian boundary on the Yangtze Platform, South China. Palaeogeogr. Palaeoclim. Palaeoecol. 274, 32–39.

Young, S.A., Saltzman, M.R., Ausich, W.I., Desrochers, A., Kaljo, D., 2010. Did changes in atmospheric CO_2 coincide with latest Ordovician glacial–interglacial cycles? Palaeogeogr. Palaeoclim. Palaeoecol. 296, 376–388.

Zhang, T., Shen, Y., Algeo, T.J., 2010. High-resolution carbon isotopic records from the Ordovician of South China: links to climatic cooling and the Great Ordovician Biodiversification Event (GOBE). Palaeogeogr. Palaeoclim. Palaeoecol. 289, 102–112.

Zhang, T., Shen, Y., Zhan, R., Shen, S., Chen, X., 2009. Large perturbations of the carbon and sulfur cycle associated with the Late Ordovician mass extinction in South China. Geology 37, 299–302.